35 mM ammonium phosphate, pH 3.8, over 50 min) to separate PtdIns-4-P from PtdIns-5-P.

Received 20 August; accepted 23 September 1997.

1. Loijens, J. C., Boronenkov, I. V., Parker, G. J. & Anderson, R. A. The phosphatidylinositol 4-phosphate 5-kinase family. *Adv. Enz. Reg.* **36,** 115–140 (1996).
2. Damen, J. E. *et al.* The 145-kDa protein induced to associate with Shc by multiple cytokines is an inositol tetraphosphate and phosphatidylinositol 3,4,5-triphosphate 5-phosphatase. *Proc. Natl Acad. Sci. USA* **93,** 1689–1693 (1996).
3. Meyers, R. & Cantley, L. C. Cloning and characterization of a wortmannin-sensitive human phosphatidylinositol 4-kinase. *J. Biol. Chem.* **272,** 4385–4390 (1997).
4. Whiteford, C. C., Brearley, C. A. & Ulug, E. T. Phosphatidylinositol 3,5-bisphosphate defines a novel PI 3-kinase pathway in resting mouse fibroblasts. *Biochem. J.* **323,** 597–601 (1997).
5. Ling, L. E., Schulz, J. T. & Cantley, L. C. Characterization and purification of membrane-associated phosphatidylinositol-4-phosphate kinase from human red blood cells. *J. Biol. Chem.* **264,** 5080–5088 (1989).
6. Bazenet, C. E., Ruano, A. R., Brockman, J. L. & Anderson, R. A. The human erythrocyte contains two forms of phosphatidylinositol-4-phosphate 5-kinase which are differentially active toward membranes. *J. Biol. Chem.* **265,** 18012–18022 (1990).
7. Auger, K. R., Serunian, L. A., Soltoff, S. P., Libby, P. & Cantley, L. C. PDGF-dependent tyrosine phosphorylation stimulates production of novel polyphosphoinositides in intact cells. *Cell* **57,** 167–175 (1989).
8. Carpender, C. L. & Cantley, L. C. Phosphoinositide kinases. *Biochemistry* **29,** 11147–11156 (1990).
9. Boronenkov, I. V. & Anderson, R. A. The sequence of phosphatidylinositol-4-phosphate 5-kinase defines a novel family of lipid kinases. *J. Biol. Chem.* **270,** 2881–2884 (1995).
10. Divecha, N., Truong, O., Hsuan, J. J., Hinchcliffe, K. A. & Irvine, R. F. The cloning and sequence of the C isoform of PtdIns4P 5-kinase. *Biochem. J.* **309,** 715–719 (1995).
11. Hinchliffe, K. A., Irvine, R. F. & Divecha, N. Aggregation-dependent, integrin-mediated increases in cytoskeletally associated PtdInsP_2 (4,5) levels in human platelets are controlled by translocation of PtdIns 4-P 5-kinase C to the cytoskeleton. *EMBO J.* **15,** 6516–6524 (1996).
12. Castellino, A. M., Parker, G. J., Boronenkov, I. V., Anderson, R. A. & Chao, M. V. A novel interaction between the juxtamembrane region of the p55 tumor necrosis factor receptor and phosphatidylinositol-4-phosphate 5-kinase. *J. Biol. Chem.* **272,** 5861–5870 (1997).
13. Zhang, X. *et al.* Phosphatidylinositol-4-phosphate 5-kinase isozymes catalyze the synthesis of 3-phosphate-containing phosphatidylinositol signaling molecules. *J. Biol. Chem.* **272,** 17756–17761 (1997).
14. Yamamoto, K., Graziani, A., Carpenter, C., Cantley, L. C. & Lapetina, E. G. A novel pathway for the formation of phosphatidylinositol 3,4-bisphosphate. Phosphorylation of phosphatidylinositol 3-monophosphate by phosphatidylinositol-3-monophosphate 4-kinase. *J. Biol. Chem.* **265,** 22086–22089 (1990).
15. Yamamoto, K. & Lapetina, E. G. Protein kinase C-mediated formation of phosphatidylinositol 3,4-bisphosphate in human platelets. *Biochem. Biophys. Res. Commun.* **168,** 466–472 (1990).
16. Graziani, A., Ling, L. E., Endemann, G., Carpenter, C. L. & Cantley, L. C. Purification and characterization of human erythrocyte phosphatidylinositol 4-kinase. Phosphatidylinositol 4-kinase and phosphatidylinositol 3-monophosphate 4-kinase are distinct enzymes. *Biochem. J.* **284,** 39–45 (1992).
17. Ishihara, H. *et al.* Cloning of cDNAs encoding two isoforms of 68-kDa type I phosphatidylinositol-4-phosphate 5-kinase. *J. Biol. Chem.* **271,** 23611–23614 (1996).
18. Serunian, L. A., Auger, K. R. & Cantley, L. C. Identification and quantification of polyphosphoinositides produced in response to platelet-derived growth factor stimulation. *Meth. Enzymol.* **198,** 78–87 (1991).

Acknowledgements. We thank G. Preswich for synthetic PtdIns-5-P, K. Hinchliffe for recombinant type II PIPK, H. Ishihara for type I PIPK cDNA, K. Ravinchandran for the GST-SHIP expression vector, R. Meyers for recombinant PI-4Kβ, A. Couvillon for preparing recombinant type I PIPK and recombinant PI-3K, and D. Fruman and C. Carpenter for critically reading this manuscript, L.E.R. is supported by The Medical Foundation–Charles King Trust. This research was supported by the NIH.

Correspondence and requests for materials should be addressed to L.E.R. (e-mail: lrameh@bidmc.harvard.edu).

Folding dynamics and mechanism of β-hairpin formation

Victor Muñoz, Peggy A. Thompson, James Hofrichter & William A. Eaton

Laboratory of Chemical Physics, Building 5, National Institute of Diabetes, Digestive and Kidney Diseases, National Institutes of Health, Bethesda, Maryland 20892-0520, USA

Protein chains coil into α-helices and β-sheet structures. Knowing the timescales and mechanism of formation of these basic structural elements is essential for understanding how proteins fold[1]. For the past 40 years, α-helix formation has been extensively investigated in synthetic and natural peptides[2–5], including by nanosecond kinetic studies[6,7]. In contrast, the mechanism of formation of β structures has not been studied experimentally. The minimal β-structure element is the β-hairpin, which is also the basic component of antiparallel β-sheets. Here we use a nanosecond laser temperature-jump apparatus to study the kinetics of folding a β-hairpin consisting of 16 amino-acid residues. Folding of the hairpin occurs in 6 μs at room temperature, which is about 30 times slower than the rate of α-helix formation[6,7]. We have developed a simple statistical mechanical model that provides a structural explanation for this result. Our analysis also shows that folding of a β-hairpin captures much of the basic physics of protein folding, including stabilization by hydrogen bonding and hydrophobic interactions, two-state behaviour, and a funnel-like, partially rugged energy landscape.

Finding protein fragments or designed peptides for the investigation of β-hairpin formation has been difficult because of instability and/or aggregation. However, NMR has revealed a significant population of β-hairpin structure in several monomeric peptides[8–14]. We have studied one such peptide[9,10] (Fig. 1). The sequence contains a single tryptophan (W43), which provides an intrinsic probe for both equilibrium and kinetic experiments. Formation of the β-hairpin is accompanied by an increase in W43 fluorescence because of its consolidation into a hydrophobic cluster with phenylalanine 52 (F52) and valine 54 (V54). By adding a dansylated lysine to the carboxy terminus of the peptide, we have used tryptophan → dansyl excitation energy transfer as an additional probe for the degree of β-hairpin structure. Equilibrium measurements with both methods have given consistent results (Fig. 2 and Methods). Using a two-state analysis, in which the peptide is either unfolded (W43 exposed to the solvent) or folded (W43 in the β-hairpin hydrophobic cluster), we obtain apparent thermodynamic parameters for the folding transition: $\Delta H = -11.6\ \mathrm{kcal\ mol^{-1}}$, $\Delta S = -39\ \mathrm{cal\ mol^{-1}\ K^{-1}}$. The population of the β-hairpin obtained at the lowest temperature studied (273 K) is ~80% (inset to Fig. 2), in reasonable agreement with the NMR determination of the β-hairpin population[10].

To study the β-hairpin kinetics we monitored the tryptophan fluorescence following nanosecond laser temperature jumps of ~15 degrees, with final temperatures in the range 288–328 K. After completion of a temperature jump from 273 to 288 K, the tryptophan fluorescence decreases in a single exponential relaxation to its new equilibrium value in which the hairpin population has decreased by ~15% (Fig. 3a). The time constant for this relaxation is 3.7 ± 0.3 μs (s.d. from 5 experiments). In the dansylated peptide, a single relaxation with the same rate is observed ($\tau = 3.5 \pm 0.5$ μs) (Fig. 3b). In this case, however, the fluorescence increases because

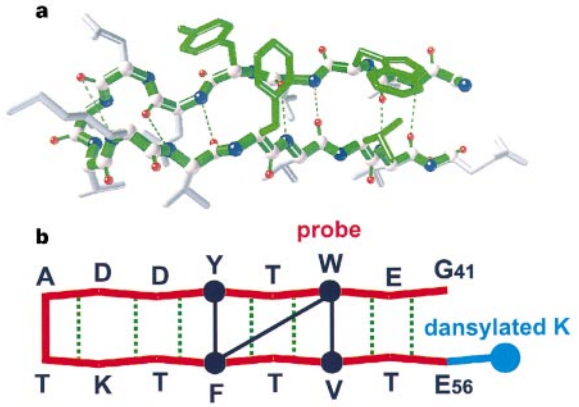

Figure 1 The β-hairpin from protein G B1. **a**, Three-dimensional structure of the C-terminal fragment (41–56) of protein G B1 in the intact protein (1GB1.PDB)[24] with the four residues of the hydrophobic cluster shown in green. **b**, Schematic representation of the structure showing the pattern of hydrogen (green) bonds and the three (blue) interactions between hydrophobic side chains that stabilize the β-hairpin structure. Observation of NOEs between the side chains of residue pairs W43-F52, W43-V54, Y45-F52 in the fragment (41–56) of protein G B1 indicate that the hydrophobic cluster is preserved in the isolated structure[10].

the average tyrptophan–dansyl distance is larger in the unfolded molecules, resulting in less quenching by Forster excitation energy transfer. The agreement in the relaxation times measured by both methods further reinforces our interpretation that the fluorescence monitors the hairpin population. It also suggests that there is a single effective thermodynamic barrier separating the folded and unfolded peptide, producing a two-state kinetic system. Assuming perfect two-state behaviour, the β-hairpin kinetics are simply described by a folding rate (with a negative activation energy) and an unfolding rate that are directly calculated from the equilibrium constants and relaxation rates at different temperatures. At the midpoint of the unfolding transition at 297 K, the folding and unfolding rates for the β-hairpin are both equal to 1/(6 μs). The rate of formation of this β-hairpin is, therefore, much slower than the rate of 1/(180 ns) recently measured for α-helix formation in a polyalanine-based helical peptide[6,7].

To explain the two-state behaviour and slower formation rate for the β-hairpin, we have developed a statistical mechanical model which grasps the structural complexity of the hairpin with a minimal number of physically meaningful parameters. The model assumes that the stability of this hairpin can be described by only three thermodynamic factors: (1) loss of conformational entropy upon fixing the peptide bonds in their native conformation (ΔS_{conf}) which opposes β-hairpin formation; (2) stabilization by backbone hydrogen bonds between the two strands (ΔH_{hb}); and (3) stabilization by the three side-chain interactions in the hydrophobic cluster (ΔG_{sc}) (Fig. 1b), which for simplicity we assume to be independent of temperature. Two possible structural states are defined for each of the 15 peptide bonds: native (native ψ of residue i, and native ϕ of residue $i+1$) and non-native (all other ψ, ϕ pairs). The number of molecular species in the model is reduced from 2^{15} (= 32,768) to 121 by assuming that there is no more than one stretch of contiguous native peptide bonds in each molecule (the single sequence approximation). The hairpin structure therefore 'grows' by adding native peptide bonds adjacent to already existing native peptide bonds. By postulating a transition state for elementary kinetic steps in which the new peptide bond already has the native conformation but no stabilizing interactions, only two additional parameters are required for a complete kinetic description of the system, an activation energy (E_0) and a pre-exponential factor (k_0). The partition function and system of differential equations describing the species population as a function of time can be readily evaluated (V.M. *et al.*, manuscript in preparation). Using the kinetic and thermodynamic constants that reproduce the experimental data, the model produces a funnel-like free energy surface[15] for the β-hairpin peptide (Fig. 4a). The prominent feature of this surface is that it contains only two global minima, and therefore a distinctly bimodal population distribution (two-state behaviour) (Fig. 4c). We identify these populations as the 'unfolded' and 'folded' states of the β-hairpin peptide. In the folded state, 99% of the molecular species contain the complete hydrophobic cluster (Fig. 1), with the most populated species having frayed ends (Fig. 4c). In spite of its kinetic complexity, the model predicts a single exponential relaxation as a consequence of a single overall free-energy barrier (Fig. 4), in agreement with our experimental results (inset to Fig. 3a). The overall transition state should correspond to the peak along the minimal free energy path (labelled ‡ in Fig. 4b). This is confirmed by the finding that only 1% of barrier crossings use alternative paths of higher free energy. The transition state species represents an ensemble of structures which contains the 45–52 stretch of native peptide bonds and all possible non-native ψ, ϕ pairs for the remaining peptide bonds. This species has a lower energy than the unfolded peptide, explaining the negative activation energy for folding in the two-state analysis. As in proteins, there is roughness in the landscape, with local free-energy barriers up to about half the size of the overall barrier (Fig. 4b).

We have also used the model (without side-chain interactions) to analyse the results obtained with laser temperature-jump experiments on a polyalanine-based helical peptide[6,7]. The model suggests that the difference between the helix and the hairpin is not in the rate of adding a new native peptide bond to the growing structure (~1 ns^{-1} for both), but is in the height of the free-energy barrier separating folded and unfolded states. In the case of helices, the

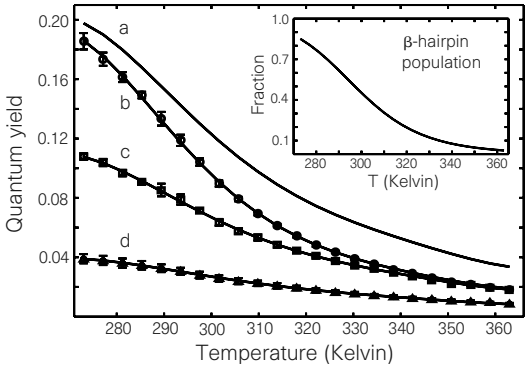

Figure 2 Thermal unfolding of the β-hairpin measured by tryptophan fluorescence (pH 7, 20 mM potassium phosphate). Curve a, calculated fluorescence of the folded hairpin. Curve b, circles, β-hairpin peptide. Curve c, squares, reference peptide GEWTY with a polynomial fit to the data. Curve d, triangles, dansylated hairpin peptide. Inset, β-hairpin population calculated from curves a, b and c. Curves b and d were obtained from fits with a two-state model (folded and unfolded). The same curves were obtained with the statistical mechanical model.

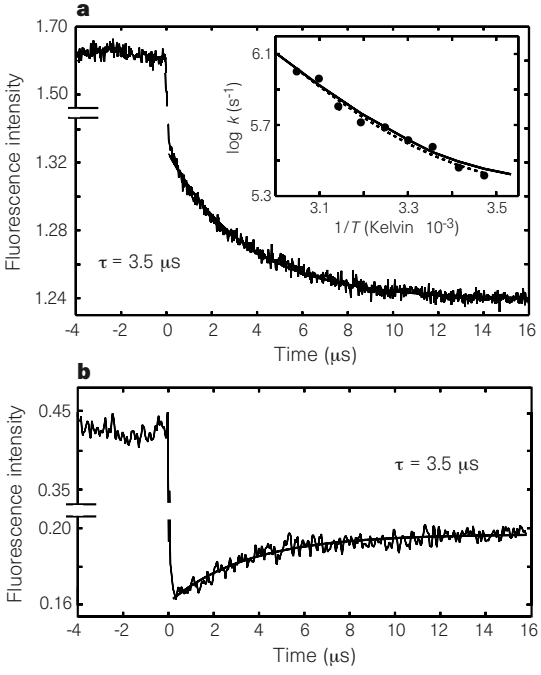

Figure 3 Kinetics of β-hairpin unfolding/refolding. **a**, W43 fluorescence of the hairpin peptide following a temperature jump from 273 K to 288 K. The initial rapid decrease is the result of a change in the intrinsic tryptophan fluorescence due solely to the change in temperature, as shown from experiments on the reference peptide (GEWTY) which shows only this fast phase. The slower phase corresponds to the unfolding and refolding of the hairpin. Inset, Arrhenius plot of the relaxation rate. The circles are the data, the dashed curve is calculated assuming a two-state model, and the continuous curve was produced by the statistical mechanical model. **b**, W43 fluorescence of the dansylated hairpin peptide following a temperature jump from 273 K to 288 K.

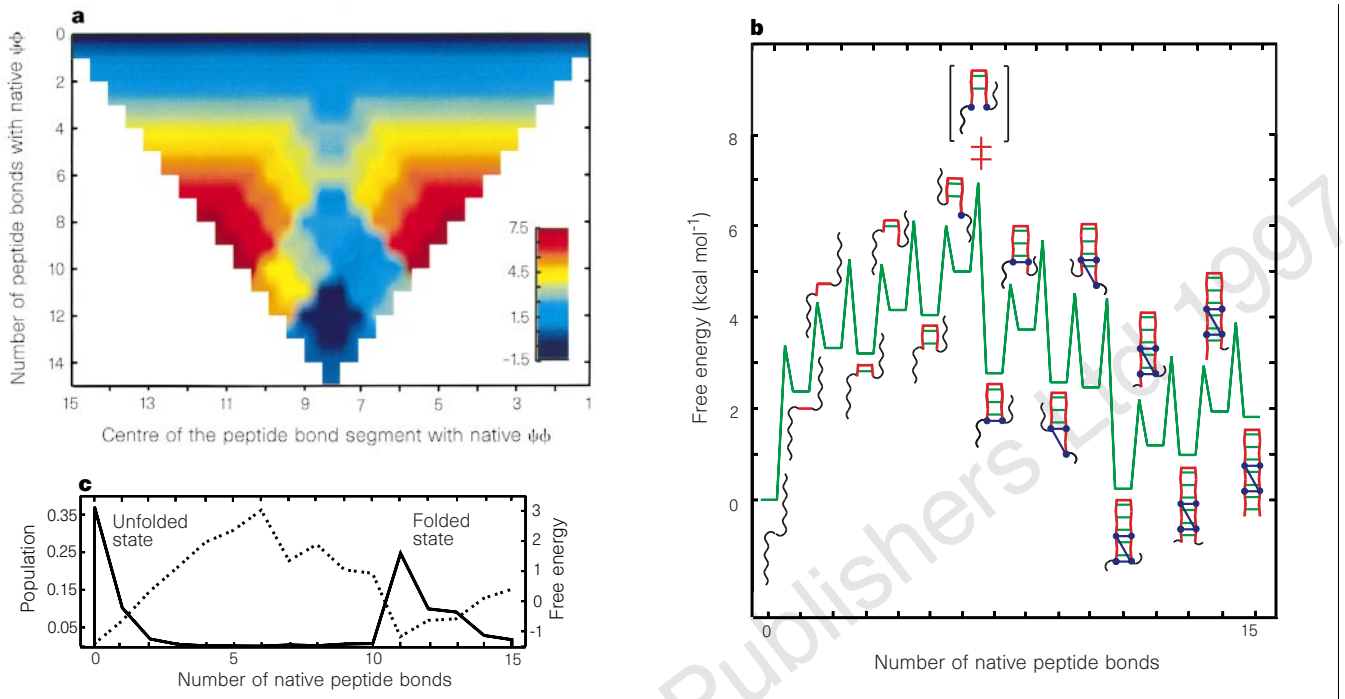

Figure 4 The free-energy landscape of the β-hairpin at the midpoint of the thermal denaturation transition. **a**, Free energy as a function of molecular conformation. Each position on the surface designates the free energy of an equilibrium molecular species, defined by the number of contiguous peptide bonds with native ψ, ϕ angles and the location in the sequence of the central native peptide bond. For clarity, the surface has been smoothed by a linear interpolation. **b**, Free energy as a function of the number of contiguous native peptide bonds along one of the two minimal free-energy paths for β-hairpin folding. The kinetic barriers between individual species are also shown. Red, green and blue lines signify native peptide bonds, hydrogen bonds and hydrophobic interactions, respectively. **c**, Equilibrium population (continuous curve) and free energy (dashed curve) as a function of the number of contiguous native peptide bonds for the hairpin.

barrier is crossed after fixing three residues in their native conformation to form the first hydrogen bond. Elongation is then thermodynamically favourable for an alanine-based helix because the entropy loss of incorporating another residue (that is, ϕ_i,ψ_i pair) into the helix is more than compensated by the energy from the new hydrogen bond. In contrast, for the hairpin, because two peptide bonds (one ψ_i,ϕ_{i+1} pair in each strand) have to be fixed to form one interstrand hydrogen bond, the process is continuously uphill in free energy until there is stabilization by side-chain interactions. The rate of hairpin formation is therefore sensitive to the position of the stabilizing residues in the sequence (for example, the model predicts that moving the tetrad of hydrophobic residues one residue towards the β turn will speed up hairpin formation by about fourfold). The second important factor in lowering the free-energy barrier and thereby producing faster rates for helices, is the larger number of productive ways of forming helices compared to hairpins. This occurs because a stretch of α-helix may form at any position along the chain with equal probability, whereas a stretch of β-hairpin structure is much less likely if it does not include the central turn region. In simulations of simple bead models using Langevin dynamics, hairpins are also found to fold more slowly, with rates surprisingly similar to the experimental values[16].

Our analysis suggests that the most probable way to initiate hairpin formation is from the β turn. However, this may be too simplistic and other mechanisms could play a role. For example, the semi-empirical estimate of 1 μs for the formation of a loop of ~10 residues[17] suggests that hairpin formation could also be initiated by loop formation to first form the hydrophobic cluster. Finally, our experimental and theoretical analysis exposes the intriguing result that a molecule as small as a 16-residue hairpin exhibits many basic features of protein folding. These include stabilization by both hydrogen bonding and hydrophobic interactions[18], two-state thermodynamics and kinetics, as found for small proteins[19], and a funnel-like, partially rough free-energy surface, as described by energy landscape theory[15]. These findings suggest that the β-hairpin is a suitable system for an in-depth study of fundamental issues in protein folding. □

Methods

Laser temperature-jump apparatus. The laser temperature-jump kinetic spectrometer, described in detail elsewhere[7,20], employs a ~4 ns Raman-shifted Nd : YAG pulse at 1.54 μm directly to heat water and an intracavity frequency-doubled argon ion laser operating at 264 nm for excitation of tryptophan fluorescence.

Materials. All peptides were >95% purity and were purchased from California Peptide Research (Napa, CA). For kinetic experiments the peptide concentration was 400 μM, which is sufficiently dilute to prevent aggregation at all temperatures studied.

Quantum yields. Quantum yields were determined by comparison with *N*-acetyl-L-tryprophanamide, taken as 0.13 at 298 K. The fluorescence of the reference peptide (GEWTY) (curve c in Fig. 2) becomes identical to that of the hairpin peptide at high temperature, and is assumed to correspond to the fluorescence of the fully unfolded hairpin peptide at all temperatures. The temperature dependence of the quantum yield for the folded hairpin (curve a in Fig. 2) was obtained by multiplying the curve for the reference peptide GEWTY by a constant that best reproduced the relative amplitudes of the fast and slow kinetic phases in the temperature-jump experiments. The fast phase in the hairpin peptide is due to the intrinsic change in tryptophan fluorescence with temperature. Its amplitude is determined by the relative populations of folded and unfolded peptide at the initial temperature, and their quantum yields at both the initial and final temperature. The amplitude of the slow phase is determined by the change in hairpin population upon increasing the temperature and the quantum yields of both the folded and unfolded peptide at the final temperature.

For the dansylated peptide the quantum yields (relative to the undansylated peptide) required to fit the equilibrium data (curve d in Fig. 2) with a two-state model were 0.21 and 0.50 for the folded and unfolded peptide, respectively. This is in reasonable agreement with the values of 0.17 and 0.71 calculated from Forster theory. In this calculation, $r_o = 2.2$ nm for the tryptophan–dansyl pair, the W43–dansyl distance was estimated as 1.5 nm for the hairpin, and a random-coil distribution with a Flory characteristic ratio of 6 was assumed for the unfolded peptide.

Fitting parameters. The temperature dependence of the observed relaxation rate (inset to Fig. 3) was fitted with a two-state model using the equation: $\ln k_{obs} = \ln[k_f + k_u] = \ln[(A \exp(-E_a/RT))(1 + 1/K)]$ with $A = 2.9 \times 10^4\ s^{-1}$, $E_a = -1\ kcal\ mol^{-1}$, and K obtained from the equilibrium data. The parameters of the statistical mechanical model used in constructing the free energy surface in Fig. 4a, as well as the curves in Figs 2 and 3, were obtained by simultaneously fitting the kinetic and equilibrium data. The resulting parameters (per bond or iteraction) are $\Delta S_{conf}(\text{hairpin}) = -3.2\ cal\ mol^{-1}\ K^{-1}$, $\Delta H_{hb} = -1.1\ kcal\ mol^{-1}$, $\Delta G_{sc} = -2.1\ kcal\ mol^{-1}$, $k_o = 1.5 \times 10^{10}\ s^{-1}$, and $E_o = 1.0\ kcal\ mol^{-1}$. The value of $3\Delta G_{sc}$ corresponds to the burial of about 300 Å^2 of nonpolar surface area in forming the 3 interactions in the 4-residue hydrophobic cluster[21,22]. It is smaller than the value of 420 Å^2 calculated from the three-dimensional structure, possibly because this calculation neglects the decrease in entropy associated with immobilizing the 4 side chains in the cluster. The same parameters were used for fitting the data on the helix[6,7], except that $\Delta S_{conf}(\text{helix}) = -2.90\ cal\ mol^{-1}\ K^{-1}$. With these parameters, the fundamental rates for the single steps of making and breaking a hydrogen bond are, respectively: $k_o \exp[(T\Delta S_{conf} - E_o)/RT] \simeq k_o \exp[(-E_o + \Delta H_{hb})/RT] \simeq 1\ ns^{-1}$. This value is consistent with the finding by time-resolved infrared spectroscopy that a decrease in β-structure hydrogen bonding in ribonuclease A occurs at 1–5 ns after a temperature jump[23].

Received 21 May; accepted 18 August 1997.

1. Eaton, W. A., Muñoz, V., Thompson, P. A., Chan, C.-K. & Hofrichter, J. Submillisecond kinetics of protein folding. *Curr. Opin. Struct. Biol.* **7,** 10–14 (1997).
2. Zimm, B., Doty, P. & Iso, K. Determination of the parameters for helix formation in poly-γ-benzyl-L-glutamate. *Proc. Natl Acad. Sci. USA* **45,** 1601–1607 (1959).
3. Gruenewald, B., Nicola, C. U., Lustig, A. & Schwarz, G. Kinetics of the helix-coil transition of a polypeptide with non-ionic side groups, derived from ultrasonic relaxation measurements. *Biophys. Chem.* **9,** 137–147 (1979).
4. Chakrabartty, A. & Baldwin, R. L. α-Helix stability. *Adv. Prot. Chem.* **46,** 141–176 (1995).
5. Muñoz, V. & Serrano, L. Helix design, prediction and stability. *Curr. Opin. Biotech.* **6,** 382–386 (1995).
6. Williams, S. *et al.* Fast events in protein folding: helix melting and formation in a small peptide. *Biochemistry* **35,** 691–697 (1996).
7. Thompson, P. A., Eaton, W. A. & Hofrichter, J. Laser temperature jump study of the helix-coil kinetics of an alanine peptide interpreted with a "kinetic zipper" model. *Biochemistry* **36,** 9200–9210 (1997).
8. Blanco, F. J. *et al.* NMR evidence of a short linear peptide that folds into a β-hairpin in aqueous solution. *J. Am. Chem. Soc.* **115,** 5887–5888 (1993).
9. Kobayashi, N., Yoshii, H., Murakami, T. & Munekata, E. *Peptide Chem.* 278–290 (1993).
10. Blanco, F. J., Rivas, G. & Serrano, L. A short linear peptide that folds into a β-hairpin in aqueous solution. *Nature Struct. Biol.* **1,** 584–590 (1994).
11. Searle, M. S., Williams, D. H. & Packman, L. C. A short linear peptide derived from the N-terminal sequence of ubiquitin folds into a water-stable non-native β-hairpin. *Nature Struct. Biol.* **2,** 999–1006 (1995).
12. de Alba, E., Jimenez, M. A., Rico, M. & Nieto, J. L. Conformational investigation of designed short linear peptides able to fold into β-hairpin structures in aqueous solution. *Folding & Design* **1,** 133–144 (1996).
13. Ramirez-Alvarado, M., Blanco, F. J. & Serrano, L. De novo design and structural analysis of a model β-hairpin peptide system. *Nature Struct. Biol.* **3,** 604–611 (1996).
14. Sieber, V. & Moe, G. R. Interactions contributing to the formation of a β-hairpin-like structure in a small peptide. *Biochemistry* **35,** 181–185 (1996).
15. Bryngelson, J. D., Onuchic, J. N., Socci, J. D. & Wolynes, P. G. Funnels, pathways, and the energy landscape theory of protein folding: a synthesis. *Proteins* **21,** 167–195 (1995).
16. Klimov, D. K. & Thirumalai, D. Viscosity dependence of the folding rates of proteins. *Phys. Rev. Lett.* **79,** 317–320 (1997).
17. Hagen, S. J., Hofrichter, J., Szabo, A. & Eaton, W. A. Diffusion-limited contact formation in unfolded cytochrome c: estimating the maximum rate of protein folding. *Proc. Natl Acad. Sci. USA* **93,** 11615–11617 (1996).
18. Kauzmann, W. Some factors in the interpretation of protein denaturation. *Adv. Prot. Chem.* **14,** 1–63 (1959).
19. Fersht, A. R. Nucleation mechanisms in protein folding. *Curr. Opin. Struct. Biol.* **7,** 3–9 (1997).
20. Thompson, P. A. in *Techniques in Protein Chemistry* Vol. VIII (ed. Marshak, D. R.) 735–743 (Academic, San Diego, 1997).
21. Baldwin, R. L. Temperature dependence of the hydrophobic interaction in protein folding. *Proc. Natl Acad. Sci. USA* **83,** 8069–8072 (1986).
22. Livingstone, J. R., Spolar, R. S. & Record, M. T. Jr Contribution to the thermodynamics of protein folding from the reduction in water-accessible nonpolar surface area. *Biochemistry* **30,** 4237–4244 (1991).
23. Phillips, C. M., Mizutani, Y. & Hochstrasser, R. M. Ultrafast thermally induced unfolding of RNase A. *Proc. Natl Acad. Sci. USA* **92,** 7292–7296 (1996).
24. Gronenborn, A. M. *et al.* A novel, highly stable fold of the immunoglobulin binding domain of streptococcal protein G. *Science* **253,** 657–661 (1991).

Acknowledgements. We thank A. Szabo and P. Wolynes for helpful discussions. We also thank J. Omichinsky for providing material used in the preliminary stages of this work. V.M. was supported by a postdoctoral fellowship from the Human Frontiers Science Program Organization.

Correspondence and requests for materials should be addressed to either V.M. or W.A.E. (e-mail addresses: vmunoz@helix.nih.gov;eaton@helix.nih.gov).

correction

K^+ channel regulation of signal propagation in dendrites of hippocampal pyramidal neurons

Dax A. Hoffman, Jeffrey C. Magee, Costa M. Colbert & Daniel Johnston

Nature **387,** 860–875 (1997)

On page 875 of this Article, there are some typographical errors in the equations used in the computer model. The errors are in the third and fourth full paragraphs on this page.

The first sentence of paragraph 3 should begin: "The Na^+ channel model was of the form, $g_{Na} = 4.2\bar{g}_{Na}m^3h$, …. The equation for α_m in paragraph 3 should read: $\alpha_m(v) = 0.182(v + 32.5)/(1 - \exp(-(v + 32.5)/4.5))$.

The first sentence of paragraph 4 should read: "The A-type channel models were of the form $g_{K_A} = \bar{g}_{K_A}m^4h$." The equation for β_h in paragraph 4 is mislabelled as β_m and the α_h equation has an incorrect minus sign. The sentence should read: "$h_{ss}(v) = \alpha_h(v)/(\alpha_h(v) + \beta_h(v))$, where $\alpha_h(v) = -0.01(v + 58)/(\exp((v + 58)/8.2) - 1)$ and $\beta_h(v) = 0.01(v + 58)/(\exp((v + 58)/-8.2) - 1)$ for all A-channels." □